Received: 5 May 2020 | Revised: 12 July 2020 | Accepted: 19 August 2020

DOI: 10.1002/eng2.12300

RESEARCH ARTICLE

WILEY

Chemical composition tuning induced variable and enhanced dielectric properties of polycrystalline $Ga_{2-2x}W_xO_3$ ceramics

Vishal B. Zade[1] | **Mohan R. Rajkumar**[1] | **Ron Broner**[2] | **Chintalapalle V. Ramana**[1]

[1]Center for Advanced Materials Research (CMR), University of Texas at El Paso, El Paso, Texas, USA

[2]Department of Physics, University of California - Santa Barbara, Santa Barbara, California, USA

Correspondence
Chintalapalle V. Ramana, Center for Advanced Materials Research (CMR), University of Texas at El Paso, 500 W University Ave, El Paso, Texas 79968, USA.
Email: rvchintalapalle@utep.edu

Funding information
Division of Materials Research, Grant/Award Number: DMR-1827745; Non-Academic Research Internships for Graduate Students, National Science Foundation, Grant/Award Number: NSF 18-102

Abstract

We report on the tunable and enhanced dielectric properties of tungsten (W) incorporated gallium oxide (Ga_2O_3) polycrystalline electroceramics for energy and power electronic device applications. The W-incorporated Ga_2O_3 ($Ga_{2-2x}W_xO_3$, $0.00 \leq x \leq 0.20$; GWO) compounds were synthesized by the high-temperature solid-state chemical reaction method by varying the W-content. The fundamental aspects of the dielectric properties in correlation with the crystal structure, phase, and microstructure of the GWO polycrystalline compounds has been investigated in detail. A detailed study performed ascertains the W-induced changes in the dielectric constant, loss tangent (tan δ) and ac conductivity. It was found that the dielectric constant increases with addition of W in the system as a function of temperature (25°C-500°C). Frequency dependence (10^2-10^6 Hz) of the dielectric constant follows the modified Debye model with a relaxation time of ~20 to 90 μs and a spreading factor of 0.39 to 0.65. The dielectric constant of GWO is temperature independent almost until ~300°C, and then increases rapidly in the range of 300°C to 500°C. W-induced enhancement in the dielectric constant of GWO is fully evident in the frequency and temperature dependent dielectric studies. The frequency and temperature dependent tan δ reveals the typical behavior of relaxation loses in GWO. Small polaron hopping mechanism is evident in the frequency dependent electrical transport properties of GWO. The remarkable effect of W-incorporation on the dielectric and electrical transport properties of Ga_2O_3 is explained by a two-layer heterogeneous model consisting of thick grains separated by very thin grain boundaries along with the formation of a Ga_2O_3-WO_3 composite was able to account for the observed temperature and frequency dependent electrical properties in GWO. The results demonstrate that the structure, electrical and dielectric properties can be tailored by tuning W-content in the GWO compounds.

KEYWORDS

chemistry, dielectric properties, gallium oxide, microstructure

1 | INTRODUCTION

Oxide dielectrics and semiconductors have been at the center of technological applications in photocatalysis, chemical sensing, energy storage, and optoelectronics for decades.[1-9] Gallium oxide (Ga_2O_3) has stood out of the transparent, wide band gap oxides and there have been demonstrated applications which utilizes its unique characteristics.[5,10-14] Among the known polymorphs of Ga_2O_3 viz. α-, β-, γ-, δ-, ε-,[15-17] β-Ga_2O_3 is the most stable. β-Ga_2O_3 has a wide band gap of ~4.9 eV which is the second only to diamond.[14,18] The electrical breakdown voltage is exceptionally high 8 MV/cm, which in comparison to SiC and GaN, 2.5 and 3.3 MV/cm, respectively, is in multiples.[13,19,20] These properties make β-Ga_2O_3 a suitable candidate for a wide variety of energy, electronic, power, optoelectronics, and catalysis applications, which include solar blind UV-photodetectors,[5,12,14,21] light emitting diodes (LEDs),[22,23] transparent conducting oxide electrodes (TCOs),[24,25] photo- and electro-catalysts,[26-28] high-temperature sensors,[29,30] high power electronic devices[11-14,31,32] with a potential to dwarf the existing SiN, Si and GaN devices in terms of performance. On the other hand, the potential for Ga_2O_3 to derive new properties and phenomena, which can facilitate designing materials especially for energy related applications, is continually evolving. Recent reports on the enhanced performance of Ga_2O_3-graphene oxide hybrid nanomaterials is a typical example that exemplifies the possibility to design new electrode materials based on Ga_2O_3 for novel electrochemical energy technologies.[33,34] Furthermore, it is proven that tailored composites, where an oxide combined with graphene sheets, causes extrinsic defects and more active sites, both resulting in the lithiation and anode stability.[34-36] Such recently discovered new phenomena assures the possibility of the design and development of novel electrode materials based on Ga_2O_3 and its composites.

Due to a wide range of applications in power electronic devices and optoelectronics related technologies, a large amount of work has been devoted to the study of the optoelectronic and dielectric properties of both intrinsic and doped Ga_2O_3 materials. It was demonstrated that the red-photoluminescence or green-photoluminescence can be derived in Ga_2O_3 by selectively doping with Cr^{3+} or Er^{3+}, respectively.[37] Recently, in view of the potential benefits of transition metal ion doping as impurities and/or inclusions into the bulk of β-Ga_2O_3, a few studies specifically attempted to understand the mechanistic aspects using theoretical studies.[18,37,38] Most important to mention were those carried out with Density Function Theory calculations, which revealed that the W, Mo and Re dopants act as deep donors in contrast to the Nb doping which acts as a shallow donor.[38] In our previous research, we directed our efforts to elucidate the fundamental science of doped and alloyed Ga_2O_3 materials, especially the design and development of materials with controlled chemical, physical and electronic properties.[3,39-42] We paid utmost attention to the tailoring the optical band gap by customizing the deposition temperature and/or fabrication method for different cations in Ga_2O_3. Sustained efforts have proved a red shift in optical bandgap as reported for W-incorporated β-Ga_2O_3[39] and Ti-incorporated β-Ga_2O_3[40] polycrystalline thin films. Detailed structural analyses of Fe-alloyed Ga_2O_3 reveal the effect of Fe^{3+} substitution in Ga^{3+} in octahedral and tetrahedral positions owing to its closeness in Shannon ionic radii.[43] A strong correlation was established between the chemical composition, crystal structure and dielectric properties with reference to the selected doping conditions and parameters.[43] In the present work, we investigate in detail and explore the properties of W-mixed Ga_2O_3 (GWO) polycrystalline compounds with a strong focus on understanding their dielectric and electrical transport properties. Interestingly, as presented and discussed in this paper, our results demonstrate that the W-content into Ga_2O_3 induces enhancement in the dielectric properties of the GWO compounds.

The existing few studies on the effect of W addition as a dopant or into the bulk of Ga_2O_3 in the literature were mostly focused on the structure and electronic properties. The attention paid toward the dielectric properties of the W-doped and/or W-mixed Ga_2O_3 polycrystalline materials are meager. For instance, studies on vacuum evaporated W-doped Ga_2O_3 films reported[44] that the W-doping influences the optical properties, where variable W% gives rise to 0.2 to 0.4 eV of red shift of bandgap and it further substantiates the effect on relaxation time due to the W incorporation. However, electrical properties of W-doped Ga_2O_3 films indicate that the doping of tungsten led to a significant decrease in the dielectric constant of Ga_2O_3 film and transformed it into a low-k insulator.[44] The chemical quality of the materials is questionable since vacuum evaporation may not be suitable to deposit high-quality oxide films with control over stoichiometry. The same author observed a monotonic increment in the red-shift of bandgap due to Ti-doping in Ga_2O_3 along with a strong dependency of capacitance, dissipation and ac-conductivity as the doping concentration increases.[45] However, similar behavior as seen for W-doping may be resulting from the lower chemical quality of materials sine it may be challenging to deposit a multicomponent thin films with such materials which makes it difficult to control stoichiometry and overall thickness.. On the other hand, recently, tungsten was proposed as a metal contact for Ga_2O_3 based power electronic devices.[46,47] However, the fundamental science and chemistry of W-interaction with Ga_2O_3 and diffusion and/or doping

effects of W into Ga_2O_3 is not well understood at this time. Therefore, understanding of the W-mixed Ga_2O_3 ceramics could be useful to predict the surface/interface diffusion and electrical properties of reaction compounds (if any) in such device applications involving W-Ga_2O_3 contacts.[46,47] Also, the GWO bulk ceramic materials with controlled structure and properties may be useful to employ them as target materials for high-quality thin film deposition using physical vapor deposition. In view of all these considerations, the dielectric properties of GWO bulk ceramics were investigated as a function of W-concentration and under variable conditions.

The present work may also contribute to the understanding of the effect of sintering behavior and chemical composition on the properties of mixed oxides or ceramic solid solutions based on Ga that is, $Ga_{2-x}M_xO_3$, where M represents a different cation. In fact, as widely reported in the literature, there have been significant efforts with a focus toward understanding various growth mechanisms and/or elucidating the effect of processing conditions on the synthesis of intrinsic and doped bulk Ga_2O_3 ceramics for a range of optoelectronic applications. It was reported that the sintering temperature strongly influences the microstructure and final density of sintered Ga_2O_3 ceramics.[48] The Ga_2O_3 ceramic targets with high density were obtained by using Ga_2O_3 micro-particles with uniform particle size, which shows promising applications for optoelectronic devices.[48] Similarly, the γ-Ga_2O_3-Al_2O_3 solid solutions derived based on the reaction mixtures exhibit high catalytic activities for selective reduction of NO using methane as the reducing agent.[49]

The annealing controlled growth optimization has been proved to grow La-doped a-GaOOH into nanostructures of α-Ga_2O_3 and β-Ga_2O_3 which has an influence on luminescence on La-doped β-Ga_2O_3 nano-spindles. A mixture of gallium oxide and silicon powders have been subjected to vapor-liquid-solid process or vapor-solid process to produce Si-doped Ga_2O_3 which are sensitive to UV/ blue intensity ration and eventually causes a decline in it.[50] Spectacular cactus-like nanostructures of β-Ga_2O_3 were grown to investigate field emission properties which made a headway due to its first time reporting for possible applications.[51] Ga_2O_3 transparent ceramics prepared by ceramic method with a controlled density and morphology were shown to exhibit excellent photoluminescence properties, which can mainly be attributed to the recombination between donors and acceptors. Ga_2O_3 transparent ceramics have promising applications as transparent conductive materials and inorganic scintillators.[52] Similarly, even the growth mechanisms for synthesizing rod-shape like β-Ga_2O_3 structures by calcination pointed to a noticeable change in the porosity and pore distribution[53] which is essential to understand the inclusion of impurity materials for a given targeted application. Therefore, we believe that the present work on sintered W-mixed Ga_2O_3 ceramics may also contribute to further advancements in the field, especially, in the light of existing efforts to the large class of mixed oxides and solid-solutions based on Ga_2O_3.

2 | MATERIALS AND METHODS

2.1 | Synthesis

2.1.1 | Materials and ingredients

After carrying out the stoichiometric calculations, $Ga_{2-2x}W_xO_3$ (GWO) compounds were synthesized by conventional solid-state reaction method. The WO_3 concentration was varied from $0 \leq x \leq 0.20$. The precursors Ga_2O_3 (99.99%) and WO_3 (99.9% purity) were procured from Sigma- Aldrich. We adopted the previously established procedures and methods to synthesize all the GWO compounds.[42] Briefly, to prepare selected GWO composition, the precursors were weighed in stoichiometric proportions according to the calculations. An agate mortar is ideal for the quantity of powders which was used to pulverize the powder with acetone as wetting media. This method gives a homogeneous mixture of the GWO compounds.

2.1.2 | Calcination and sintering

The homogeneous mixture of GWO powders were then transferred into crucibles and calcined at 1050°C, 12 hours and 1150°C, 12 hours in a muffle furnace. Each calcination was followed by intermediate grinding to ensure and assist the solid-state reaction. After the final calcination, the powders are thoroughly ground to enhance sinterability. The addition of polyvinyl alcohol (PVA) at this step is to give binding strength to the pulverized powder which is followed by pelletization into circular disc shape of 8 mm diameter and ~1 mm thickness. A uniaxial hydraulic press was used to apply 1.5 ton of load for this process. These green pellets were then sintered at 1250°C for 6 hours with a ramp rate of 5°C/min, and binder

burnout of pellets was ensured by holding at an intermediate temperature (500°C) for 30 minutes. The crystal structure, surface chemistry and chemical composition of all the synthesized GWO compounds are thoroughly established.[42]

2.2 | Methods

2.2.1 | Dielectric measurements

Dielectric measurements were performed using a HIOKI IM3536 LCR meter. Circuit corrections were made to ensure the accuracy of the readings taken on the LCR meter. The sample pellets were prepared by fine polishing and coating with silver paste on both sides prior to measurement. The capacitors fabricated using the GWO as dielectric while silver (Ag) serves as the metal electrodes of the capacitor. The silver coated GWO pellets were cured at 90°C for 2 hours to ensure the proper functioning of the electrodes. The capacitance, dielectric dissipation (tan δ) and inductance data were collected between 1 kHz and 1 MHz frequency (at 125 frequencies) and a temperature range of 30°C to 500°C (for every 10°C). It is well known that the electrical energy stored in a capacitor is function of capacitance, which is determined by the capacitor geometry and the dielectric constant of the oxide.[47,54-56] Thus, the dielectric constant of a material represents the charge storage capacity when a potential is applied to it.[47,54-56] It is calculated by the following equation, where the capacitance is given[47,56] by:

$$C = \varepsilon_0 \frac{A}{d}, \tag{1}$$

where, ε is the dielectric constant of the material under investigation, C represents the capacitance, A the area of the capacitor's plate, d the distance between the capacitor's parallel plates, and ε_0 the dielectric constant of free space.

3 | RESULTS AND DISCUSSION

3.1 | Dielectric constant - frequency dependence

The sintered GWO pellets were subjected to a frequency sweep ranging from 1 kHz to 1 MHz and the data obtained are shown in Figure 1. As it can be seen from Figure 1, the dielectric constant (ε') at lower frequency range shows comparatively higher values. However, as the frequency increases, the ε' then decreases. It decreases until it plateaus out with the increase in frequency. This behavior of ε' with respect to frequency is typical for all the GWO compounds. The dielectric dispersion of any dielectric material is a complicated function of the frequency of applied electric field. It also depends on the microstructure (eg, grain size) of the material system under investigation. As reported elsewhere, the incorporation of W into Ga_2O_3 results in microstructural changes.[42] Initially, the pristine Ga_2O_3 exhibits a rod-shaped structure. The addition of small quantities of W into the system changes the morphology to spherical and as the W concentration increases the grains become faceted with square or hexagonal features. The facets even exhibit twin lamellae which are unique to the GWO system. Overall the grain growth is abnormal and is attributed to the unreacted phase that is accumulated at the grain boundaries. Also, the presence of twin lamellae is due to the WO_3 which enhances the diffusion of vacancies. The fact that this abnormal grain growth with twin lamellae is contributing to the increase in grain boundary area which is assisted with the unreacted WO_3 aggregated at the grain boundaries. This overall phenomenon is contributing to the increased resistance at grain boundaries which impairs conductivity.

It is evident from Figure 1 that the real part of the dielectric constant, ε', shows usual behavior with alternating frequency. Which can be explanied by addressing the polarization source in the system.[57,58] At the lower end of the frequency range, ε' assumes higher values throughout the sweep profile. This is due to the fact that ionic, space charge and grain boundary polarization contribute to the higher values of ε' at lower frequencies.[58,59] Perhaps, the presence of space charge polarization at the grain boundaries, may generate a potential barrier. Then, an accumulation of charge at the grain boundary occurs leading to higher values of the dielectric constant.[59,60] However, it may be noted that as the frequency increases, the ε' values deccreases rapidly. This can be attributed to the species that are contributing to the polarization phenomenon, lag behind the applied voltage in the high frequency domain. This typical dielectric behvaior can be elaborated by the dispersion due to Maxwell-Wagner polarization,[61] which is corroborated by Koop's Phenomenological Theory.[62]

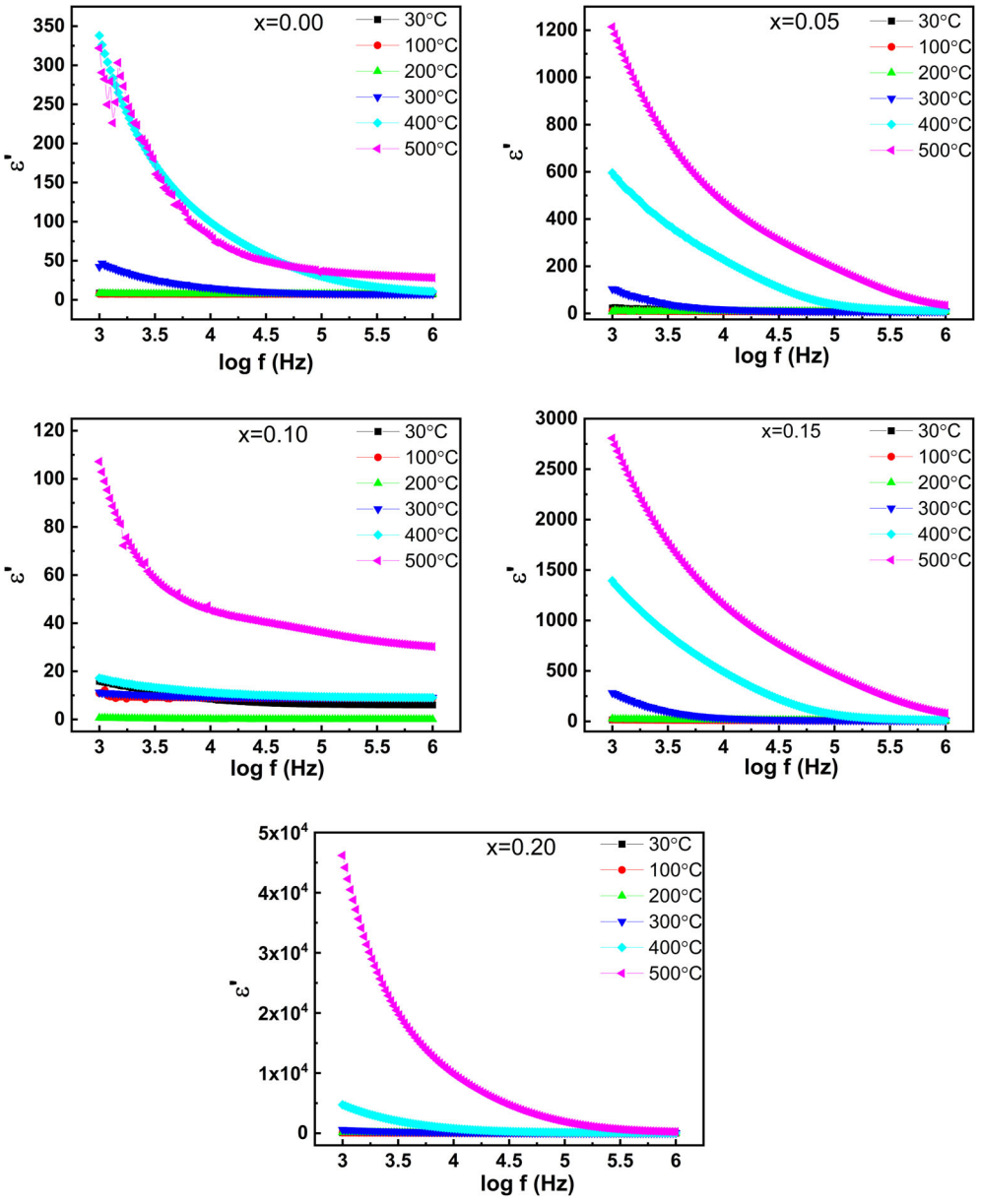

FIGURE 1 Frequency dependence real part of dielectric constant of GWO ceramics with variable W concentration. The data shown are for: A, $x = 0.00$; B, $x = 0.05$; C, $x = 0.10$; D, $x = 0.15$; and E, $x = 0.20$

Since the ceramic system in context exhibits multiple species viz. Ga^{3+}, O^{2-}, W^{3+}, it is worth employing Debye Model[63] to further understand the W-doped Ga_2O_3 system. Figure 2 shows the dielectric dispersion behavior for GWO materials using the modified Debye function as shown in the following equation[59,60,62,64]:

$$\varepsilon'(\omega) = \varepsilon_\infty + \frac{(\varepsilon'_0 - \varepsilon'_\infty)}{[1 + (\omega\tau)^{2\,(1-\alpha)}]}, \tag{2}$$

where $\varepsilon'(\omega)$ gives the complex permittivity, $(\varepsilon'_0 - \varepsilon'_\infty)$ gives the dielectric relaxation strength, ε'_0 represents the low frequency permittivity (static) while ε'_∞ represents high frequency permittivity. ω is the angular frequency which is derived from the linear frequency (f) of the applied electric field as $\omega = 2\pi f$. τ represents the Debye average relaxation time while α denotes the spreading factor of actual relxation time about the mean value.

The intrinsic paramters of the GWO compunds were determined using Cole - Cole plots[65] as can be seen in Figure 3. The values for spreading factor "α" and relaxation time "τ" were obtained by plotting ln $[(\frac{(\varepsilon'_0 - \varepsilon'_\omega)}{(\varepsilon'_\omega - \varepsilon'_\infty)}]$ as a function of ln ω with only the real part of the dielectric dispersion in context. In other words, the pioneering work of Cole-Cole with the standard procedure[65] were adopted to fit the experimental data, based on the real part of the dielectric constant instead of the complex part of the dielectric constant, and to obtain information on the dielectric relaxation behavior.[60] As reported

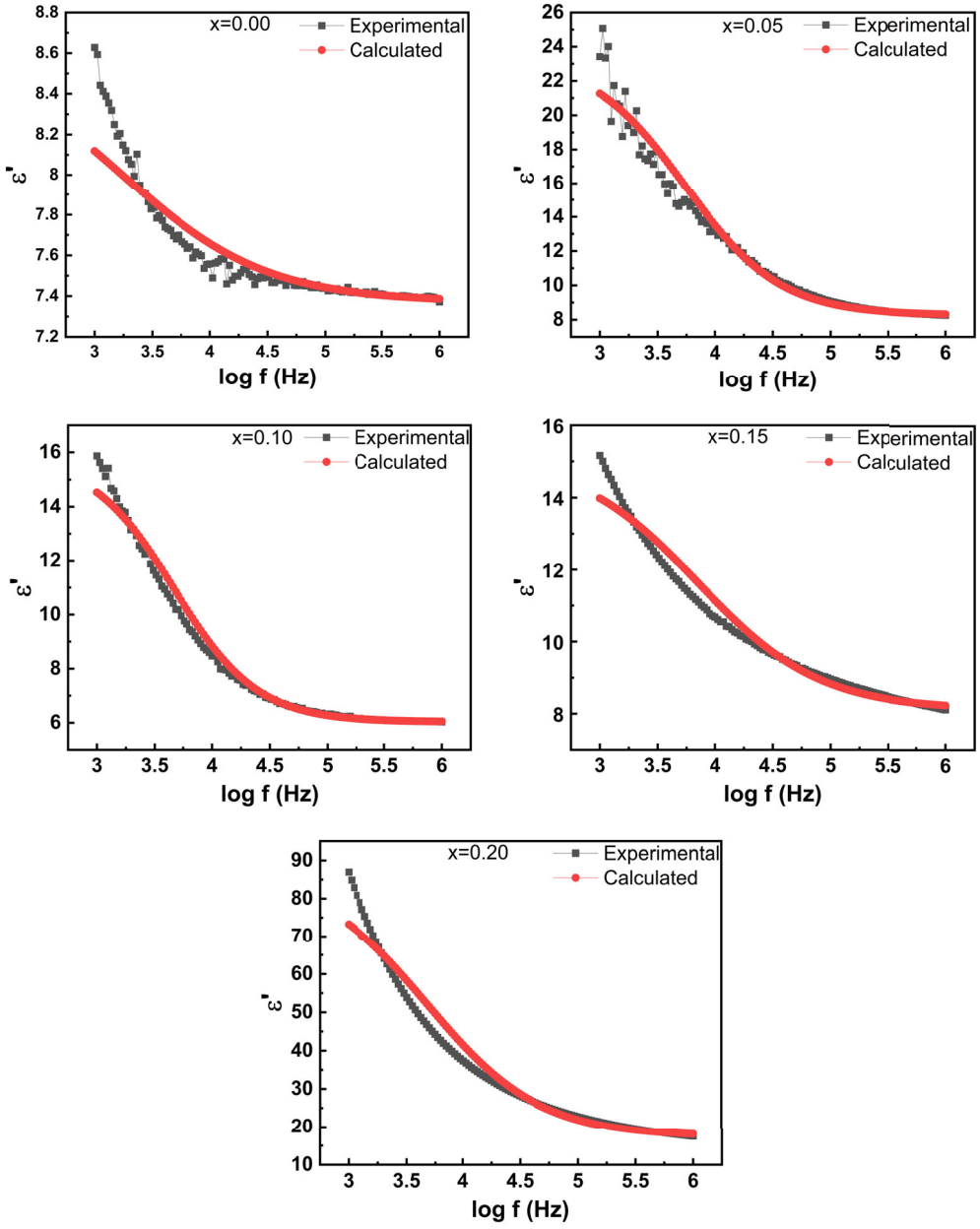

FIGURE 2 Real part of dielectric constant fitted to modified Debye Function. The plots are for different compositons of GWO

elsewhere, such analyses and procedures were found to be quite useful to understand the dielectric relaxation behavior in complex ceramics or chemical compounds with multivalent cations present.[54,55,60] The values obtained for α and τ were used to fit the data by computing the Debye function mentioned in Equation (1) and fitting it with the experimentally measured values for ε' at room temperature. As it can be seen from Figure 2, the experimental and calculated values show a good agreement which further corroborates the validity of the modified Debye's function in claiming the multiple ion contribution to the relaxation process. The α and τ values determined are tabulated in Table 1. It can be noted that these values are in reasonable agreement with doped semiconductors and complex ceramic compounds.[54,55,60]

3.2 | Dielectric constant - temperature dependence

The variation of ε' with temperature is shown in Figure 4. The data shown are for GWO compounds with variable W-content and measured at different frequencies. At lower frequency (1 kHz-10 kHz), polycrystalline β-Ga_2O_3 shows a single relaxation peak at ~400°C. The peak intensities fade at higher frequencies with no relaxation peaks at $f = 100$ kHz to 1 MHz. The inclusion of W in β-Ga_2O_3 changes a few dynamics in terms of relaxation peaks. At lower frequencies,

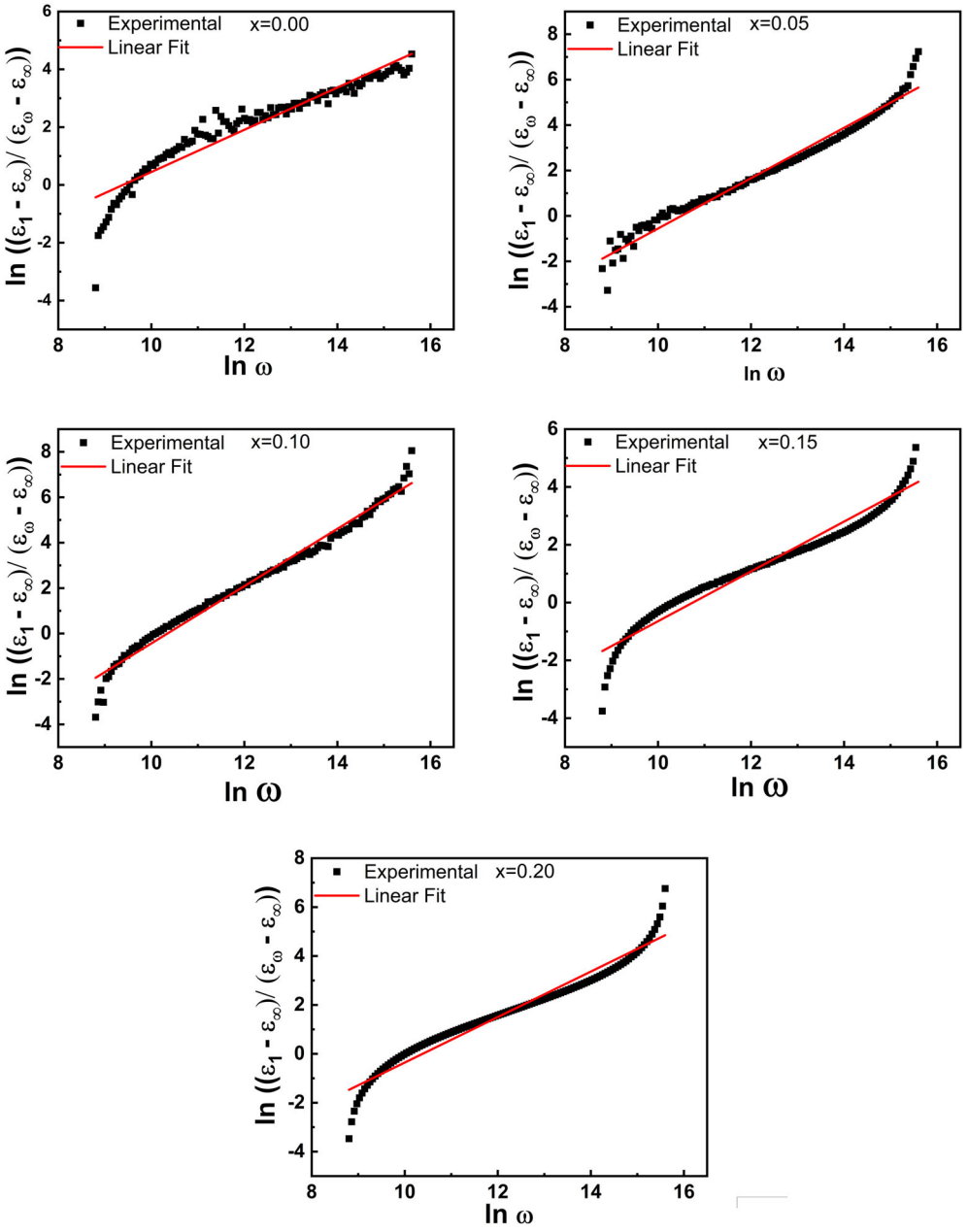

FIGURE 3 Cole - Cole plot for determining the spreading factor and relaxation time for GWO compounds. The linear portion of the fitting is used to calculate the parameters

TABLE 1 Spreading factor and relaxation time determined using Cole-Cole plots for GWO compounds

W-concentration in GWO (*x*)	Spreading factor, α	Relaxation time, τ (μs)
0.00	0.6520	91.762
0.05	0.4718	29.067
0.10	0.3991	34.126
0.15	0.5895	22.492
0.20	0.5571	32.817

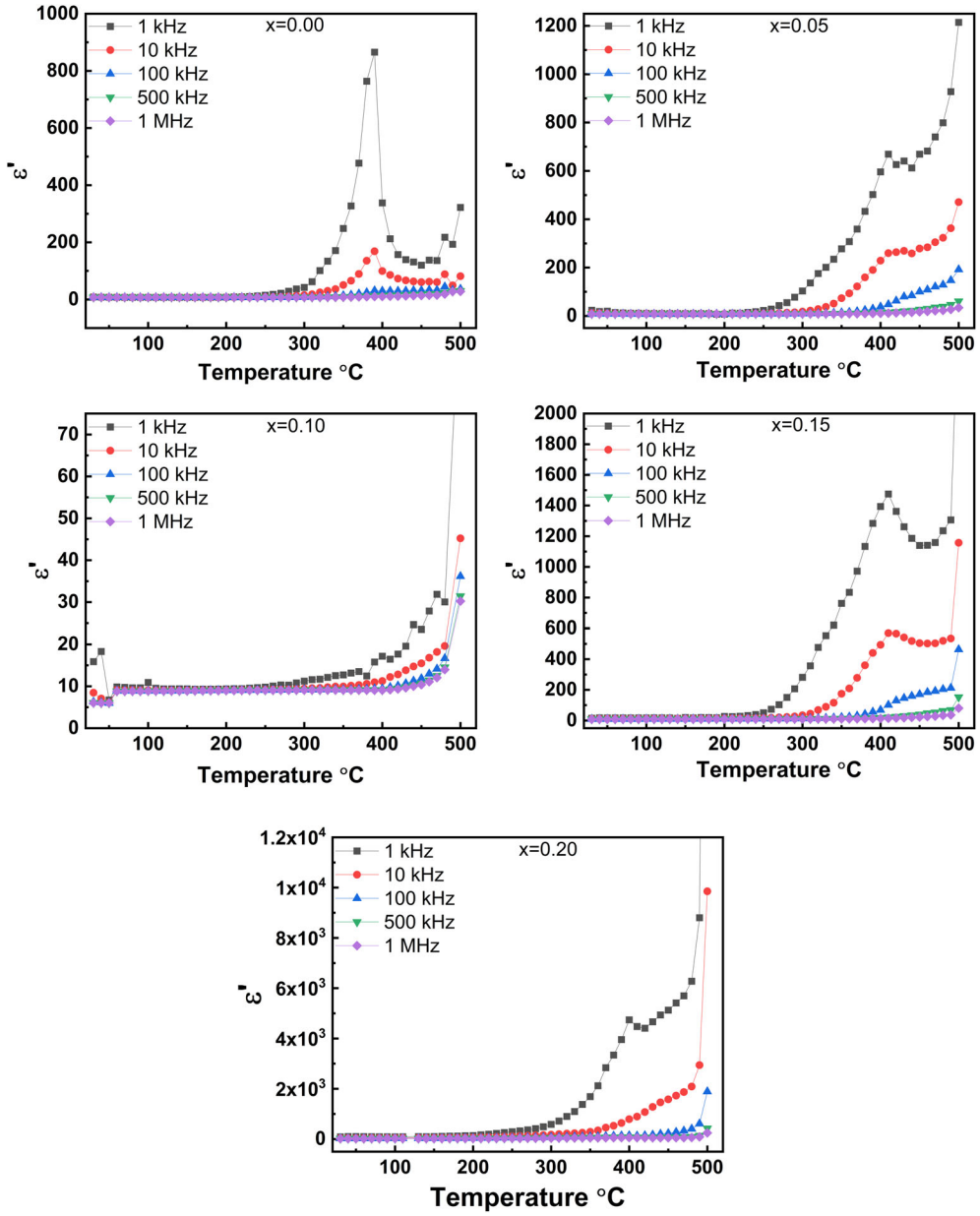

FIGURE 4 Temperature dependence of ε' in GWO compounds. The data shown are for GWO compounds with variable W-concentration (x)

almost all the GWO composites show a relaxation peak and the dielectric constant follows an increasing monotonic function. The high intensity relaxation peaks observed in β-Ga_2O_3 are due to the conduction between the grains and grain boundaries. As the W concentration in β-Ga_2O_3 increases, more and more W^{6+} ions are introduced into Ga_2O_3 altering the grain morphology from rod shaped (un-doped Ga_2O_3) to spherical shape which provides a larger area for conduction and hence the reduced intensity of relaxation peaks. Note that the dielectric properties of ceramics are highly dependent upon the microstructure, defect structure, type of ionic dopants, and temperature.[4,55,60,65,66] In fact, realizing that the energy storage properties mainly depends on the defect chemistry of the dielectric, several research groups have paid attention recently to tailor the multilayered materials for significant enhancement of energy storage performances by regulating the dielectric contrast between adjacent layers.[4,66] In the present case, as the W^{6+} substitution increases in β-Ga_2O_3, the microstructural properties are altered as evident in our previous work as well as the TEM analyses discussed in subsequent sections. Owing to the smaller ionic radius of W^{6+}, when it substitutes for Ga^{3+} (larger ionic radius), there is a shrinkage of the unit cell volume. This shrinkage results in enhanced charge carrying capability which in turn reduces the hopping distance. At $x = 0.10$, the dielectric relaxation is unnoticed but as the concentration increases, the low intensity relaxation peaks resurface. This phenomenon is attributed to the undissolved WO_3 agglomerated at the grain boundaries and increasing the resistance at interface. The abnormal grain growth arising due to vacancy assisted enhanced mass

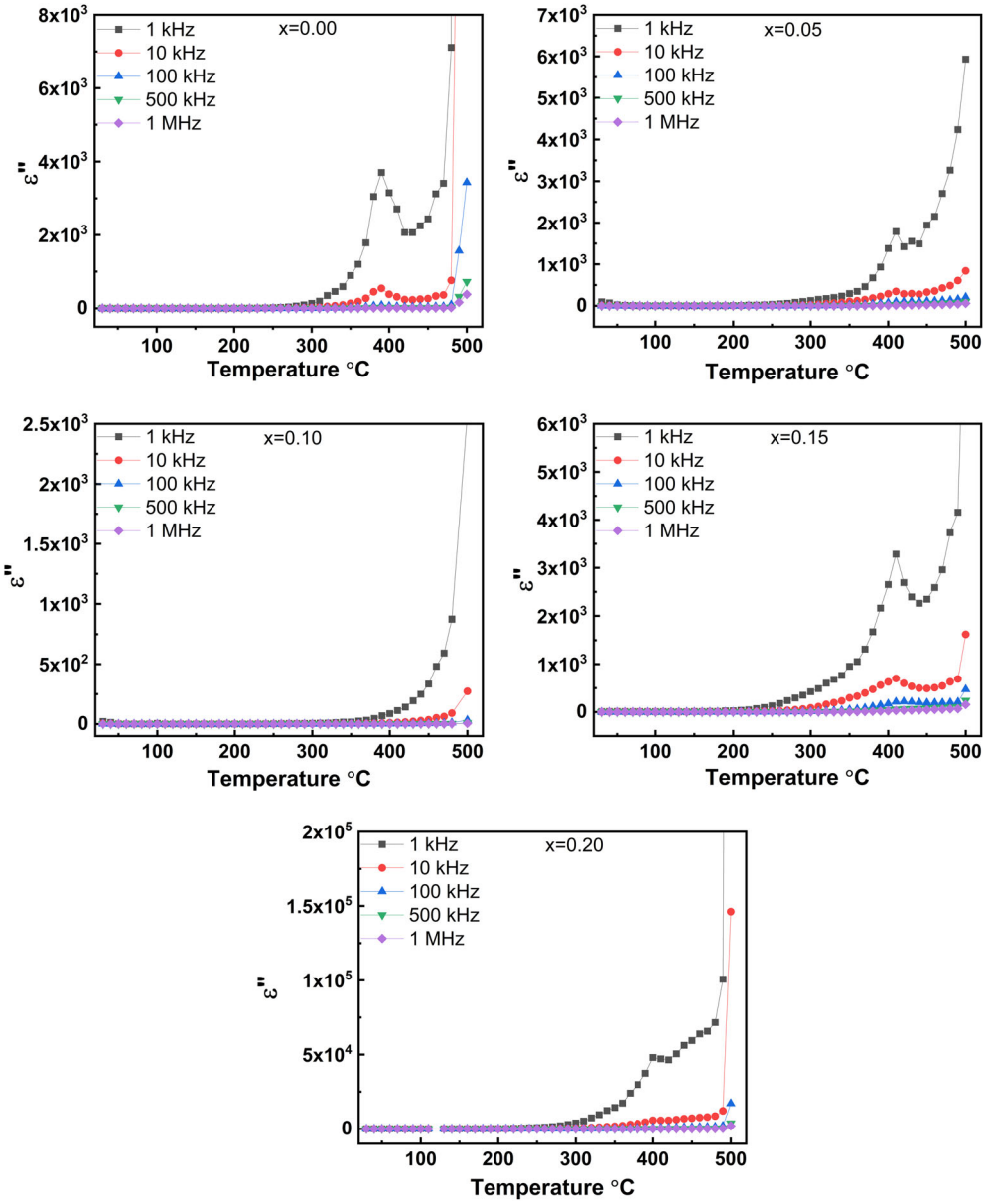

FIGURE 5 Temperature dependence of ε'' in GWO compounds as a function of frequency at different W concentration

transport is also contributing to the twin lamellae which explains the resurfacing relaxation peaks as $x > 0.10$. Thermal energy enhanced charge carrier mobility and improved hopping is generally observed at higher temperature. Thus, an increase in dielectric polarization contributes to the increased ε' values.

The temperature dependence of the corresponding imaginary part of dielectric constant for GWO compounds is presented in Figure 5. The data presented are for GWO compounds with variable W-content and measured at various frequencies. It may be noted that as WO_3 concentration increases in the system, the value for ε'' also increases. It can be seen that there is a shift in the dielectric values due to the change in temperature. This is due to the increase in charge carrier mobility and the enhanced hopping rate due to increased temperature. The lower temperature does not support this phenomenon and hence the lower values of ε''.

The frequency dependence of the corresponding imaginary part of dielectric constant for GWO compounds is presented in Figure 6. The data presented are for GWO compounds with variable W-content and measured at various temperatures. It is evident that the ε'' values tend to be generally higher at lower frequencies but decreases rapidly with increasing frequency. On the other hand, ε'' is seen to increase with increasing temperature. Also, the data clearly indicates that the temperature dependence of ε'' is strongly dependent on the frequency of measurements. These variations can be understood if we consider the microstructure variation and interfacial contributions in the W-doped Ga_2O_3 materials. The contribution of the interfacial losses and the loss from electrical conductivity (as discussed in the subsequent

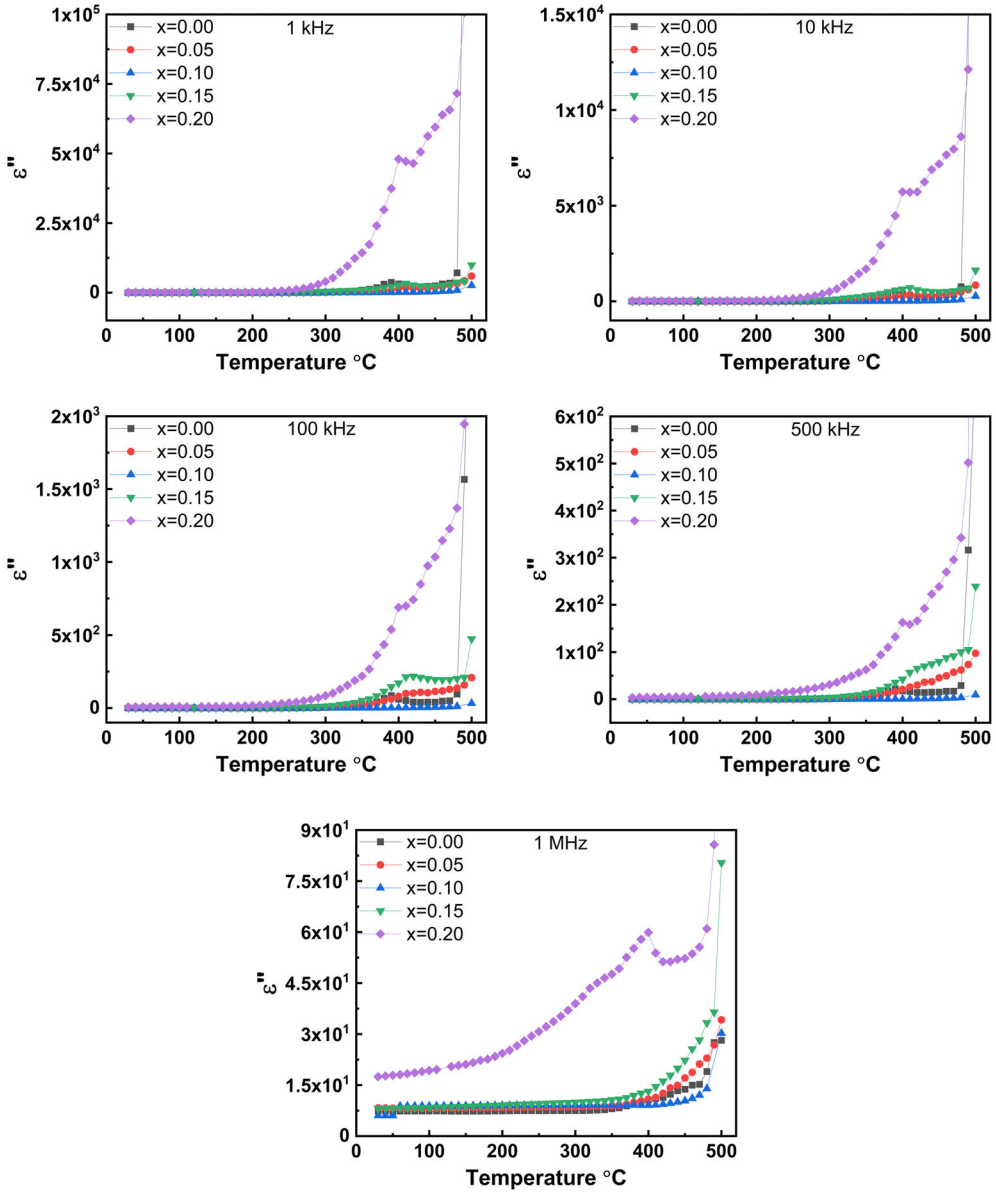

FIGURE 6 The dependence of ε'' in GWO compounds as a function of W concentration at a particular frequency

sections) is generally dominant at lower frequencies; however, these factors becomes negligible at higher frequencies.[55-59] Thus, the observed decrease in the imaginary part of the dielectric constant observed at higher frequencies can be attributed to the rapidly fading off the contributions from the interfacial as well as grain conductivity mechanisms. However, the large values - observed at lower frequency is mainly due to the W-doping induced complex chemistry of Ga_2O_3 in terms of multiple valence cations, vacancies, and grain boundary defects.[55,57-59]

3.3 | Dielectric loss

The commonly referred dielectric loss factor is defined as the ratio of imaginary part of dielectric constant to the real part and it is given by $\tan \delta = \varepsilon''/\varepsilon'$, where δ is the phase difference between current and voltage of the applied electric field.[57,63] As shown in Figure 7, the loss factor with reference to change in temperature indicates that β-Ga_2O_3 assumes a lower value for lower frequencies until temperatures of 350°C to 420°C. Then the loss $\tan \delta$ rises exponentially toward the higher range of measuring temperatures. This is true for higher frequency range as well, indicating a dormant behavior of the participating species. β-Ga_2O_3 is known to have intrinsic oxygen defects leading to space charge polarization which exists during the entire temperature sweep. As the temperature increase, this effect becomes predominant and the loss $\tan \delta$ rises exponentially as seen in Figure 7.

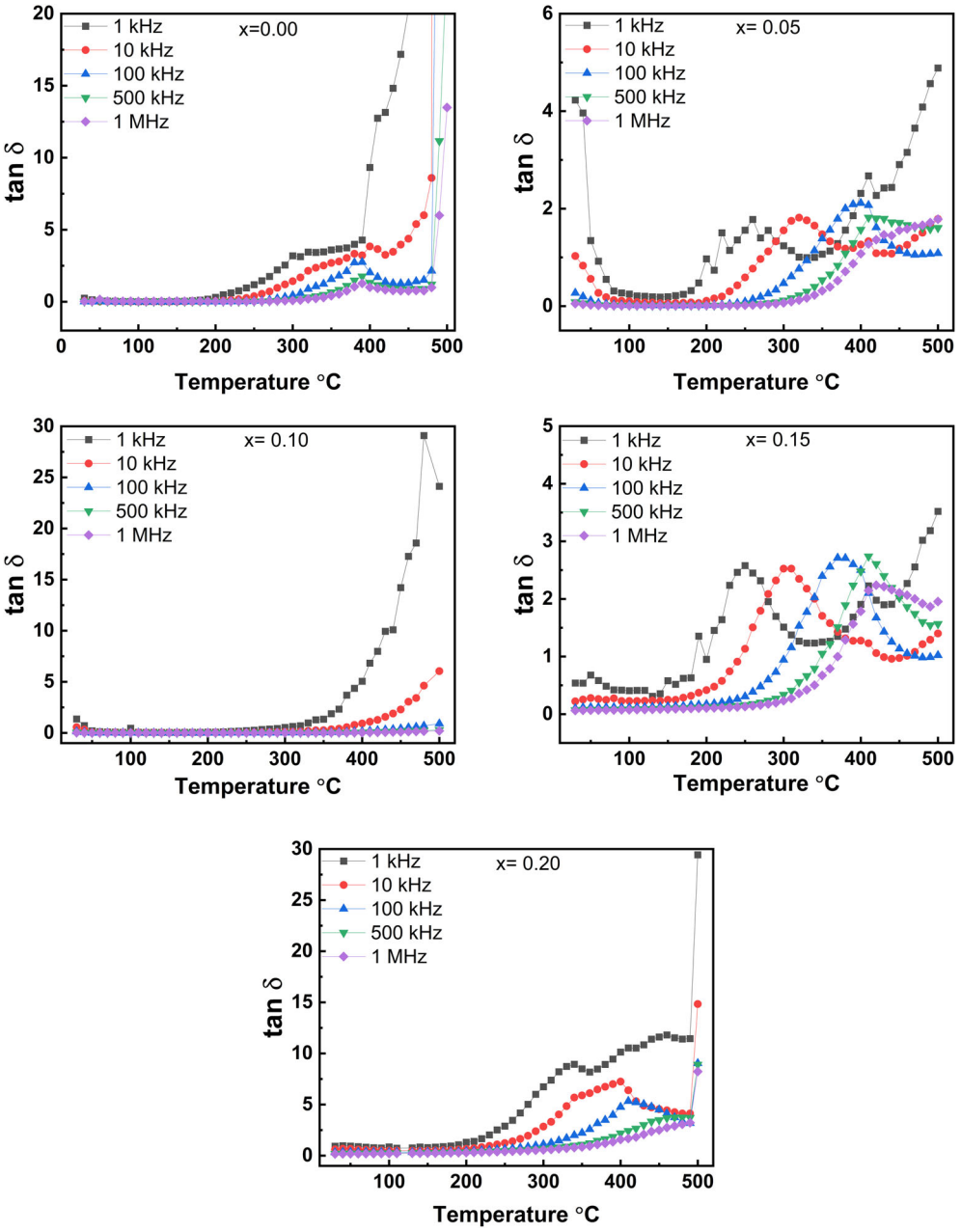

FIGURE 7 Frequency dependent dielectric loss (tan δ) of GWO compounds. The data shown are for GWO with variable W concentration and as a function of temperature

Figure 8 shows the variation of tan δ with temperature at different frequencies, it may be noted as the concentration of WO_3 in the system increase, tan δ increases. As reported elsewhere, a mixture of W^{4+} and W^{6+} valence states is present at lower W concentrations.[67] This gives rise to a charge imbalance which explains the substitution of Ga^{3+} ions and with free W ions for conduction reducing the dielectric loss at lower concentrations. With the increment in WO_3, the aggregation of mixed phase may give an improved mass transportation assisted Ga^{3+} substitution. This may finally result in a certain amount of dopant infusion and additional amount to agglomerate.

3.4 | AC conductivity

Figure 9 shows the ac conductivity of GWO samples as a function of ln ω. It is evident from the figure that the conductivity increases with the increase in frequency. It can also be seen that the conductivity increases with the increase in W content in the GWO system. This is attributed due to the electron hopping between various cations. This is also influenced by the increase in frequency which increases the hopping rate and hence the improved ac conductivity.

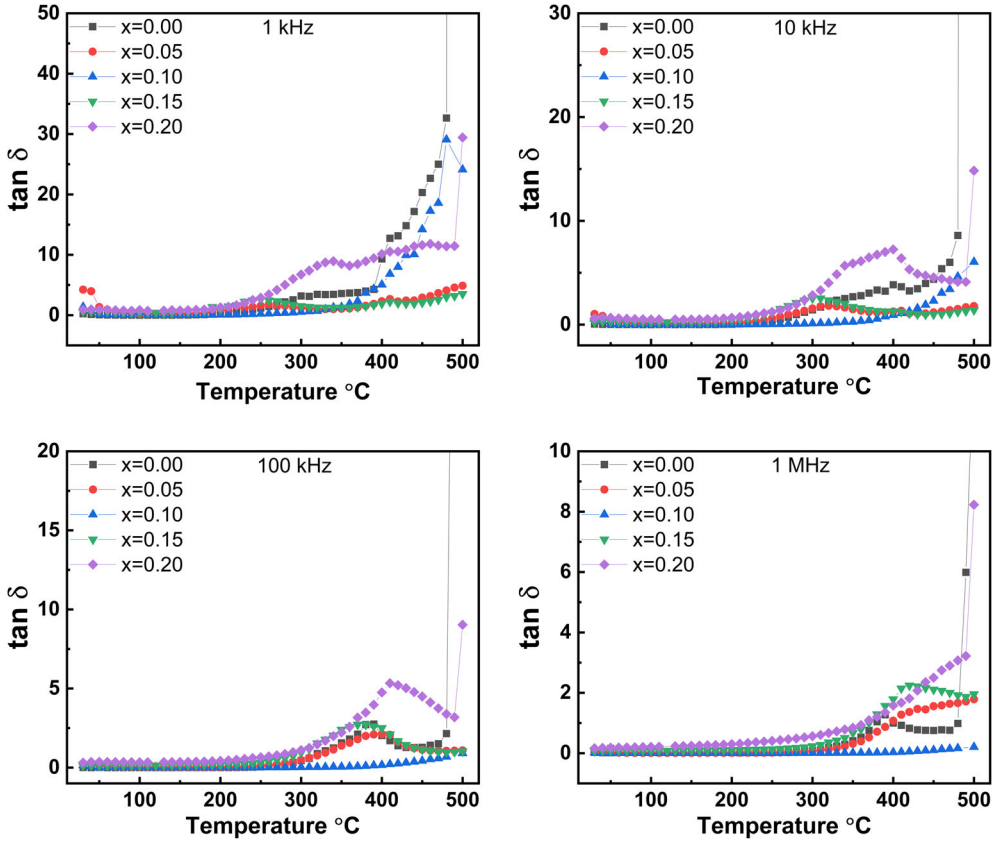

FIGURE 8 Temperature dependent dielectric loss (tan δ) of GWO compounds. The data shown are for GWO with variable W concentration and as a function of temperature

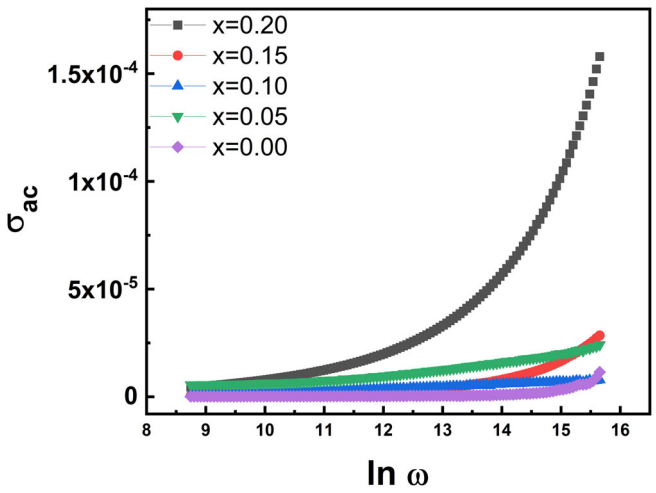

FIGURE 9 ac conductivity of GWO compounds. The frequency dependence of conductivity is presented for various GWO compositions. The data is obtained is room temperature measurements while varying frequency

To further expand the understanding of transport mechanism in GWO dielectric, a plot of σ_{ac} - σ_{dc} in log scale has been plotted against the log ω^2 as shown in Figure 10. The plots obtained validate the polaron hopping conduction mechanism involved in all the GWO dielectric materials. The polaron is often described in context of a deformable polar medium as a self-stablilized electronic charge. The lattice distortion induced slow motion in the polarons is known as polaron hopping.[55,68,69] As it can be seen in Figure 10, the W-doped Ga_2O_3 ceramics exhibit a linear growth before being achieiving the saturation state at higher frequency. Intrinsic Ga_2O_3 has the lowest magnitude as compared to other doped GWO samples which forms a cluster as the dopant level increases. The underlying mechanism behind this can be explained the following equation[68,69]:

$$\sigma_{ac} - \sigma_{dc} = \frac{\omega^2 \tau}{1 + \omega^2 \tau^2}, \tag{3}$$

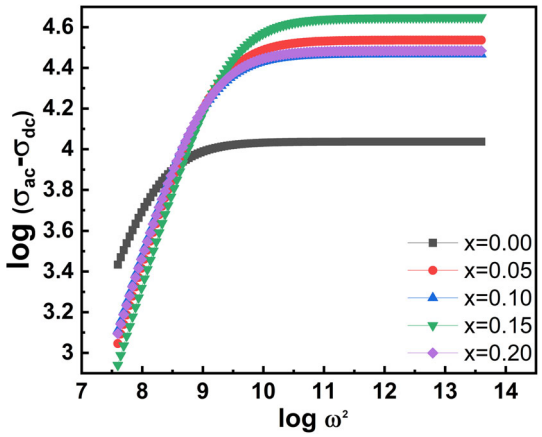

FIGURE 10 The log($\sigma_{ac} - \sigma_{dc}$) vs log ω^2 plots for GWO dielectric materials. The data shown are for GWO dielectrics with variable W-concentration. The initial linear plots are evident of small polaron hopping mechanism (see text) operative in the electrical transport properties of GWO dielectrics. The elevated set of data with a different linear behavior and slope can be also noted for W-doped vs intrinsic Ga_2O_3

where, ω is angular frequency and τ represents the average relaxation time. It is worth noting that for conduction occurring in a localized neighborhood with a small polaron hopping, $\omega^2\tau^2 < 1$, the log ($\sigma_{ac} - \sigma_{dc}$) vs log ω^2 will always represent a linear behavior which is clearly evident in Figure 10. While this observation clearly supports the fact that the electrical transport mechanism in GWO materials is based on the polaron hopping among the localized sites, the W-induced distortion of the lattice is the source of such localization of charge carriers leading to the polaron formation. Furthermore, metal-doping induced lattice distortion leading to such localization of charge carriers leading to polaron formation and polaron-hopping in the localized states facilitated electrical conduction mechanism was noted and reported in some of the doped ferrite semiconductors.[55,70-72]

3.5 | Proposed mechanism and model

Finally, based on the observations made from previously reported structural details[42,67] and the present work on frequency and temperature dependent dielectric constant, dielectric loss, and ac electrical transport analysis, the effect of W-doping on the electrical conduction mechanism and dielectric properties of Ga_2O_3 can be modelled simply from the microstructure and heterogeneity perspective. First of all, it must be emphasized that crystal structure, phase and microstructure analyses using X-ray diffraction (XRD), scanning electron microscopy (SEM) indicate that the W-doping induced changes are significant.[42,67] As reported previously, XRD analyses of GWO reveal the formation of a solid solution at lower concentrations W ($x \leq 0.10$) while unreacted WO_3 secondary phase formation occurs at higher concentrations ($x > 0.10$). Insolubility of W at higher concentrations ($x \geq 0.15$) leading to a Ga_2O_3-WO_3 composite formation is attributed to the difference in formation enthalpies of respective oxides that is, Ga_2O_3 and WO_3. Furthermore, the surface chemistry and electronic structure analyses using X-ray photoelectron spectroscopy (XPS) analyses also supported the formation of Ga_2O_3-WO_3 composite formation.[67] However, XPS studies reveal the lower valence state (W^{4+}) formation for GWO compounds with lower concentration of W, Thus, the structural and chemical analyses strongly support the idea of an heterogeneous and electronically differently characterized bilayer system for W-doped Ga_2O_3. Such simple two-layer or heterogeneous model can be formulated to account for the frequency and temperature dependent dielectric properties and electrical conduction mechanism in GWO materials. Formation of grain-interior and grain-boundary in GWO dielectric can be treated as a heterogeneous system as schematically presented in Figure 11. The proposed model contains grains of Ga_2O_3 and the secondary phase of WO_3, which may be nucleating and located more at the grain boundaries.

We hypothesized the variation in dielectric constant is a result of the formation of heterogeneous system based on the Ga_2O_3-WO_3 composite with the gradual increase in W content. Although the electrical response of the grain and grain boundaries is entirely different, the grains are essentially separated by a thin layer of grain-boundaries. It is evident from Figure 11B,C that the effect of W-content on the dielectric constant of GWO samples is remarkable. The dielectric constant increases with increasing W-content and is attributed to the lattice distortion of the intrinsic Ga-oxide which is in-turn the result of enhanced atomic polarizability. Additionally, formation of a small amount of WO_3 leads to the heterogeneous system which presents itself as WO_3 phase at the grain boundaries leading to the accumulation of charges at the grain boundaries. The resulting interfacial polarization further contributes to an increase in dielectric constant. This would also explain the ac conductivity of the GWO dielectrics. At lower frequencies, the grain boundaries are highly

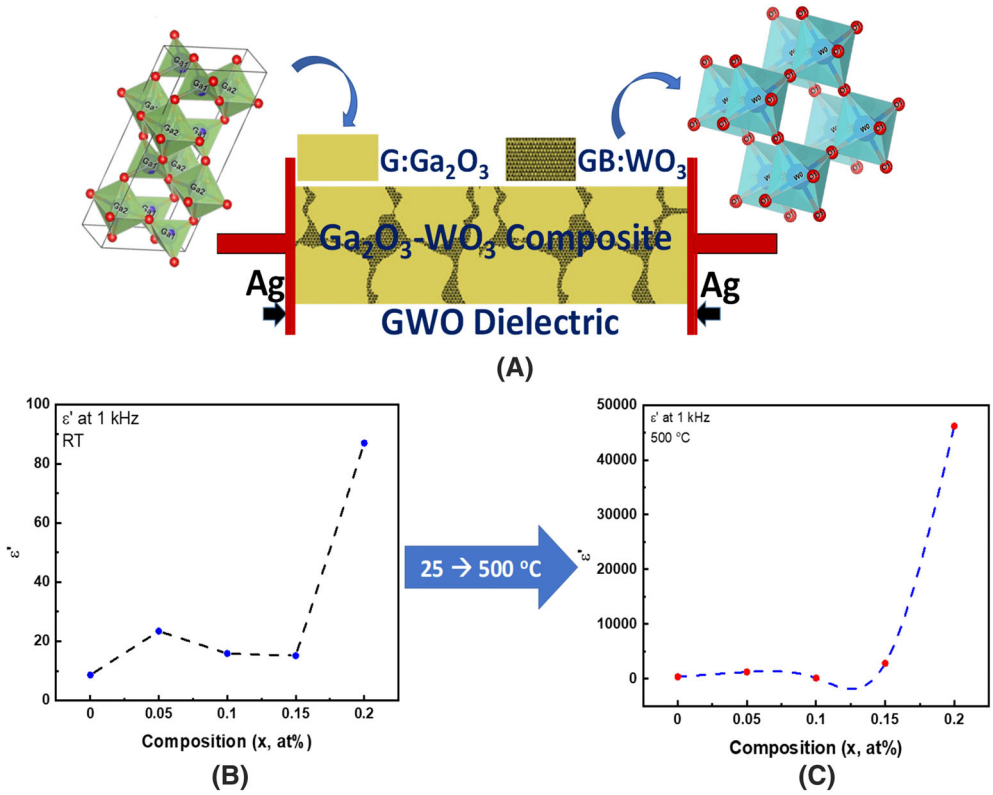

FIGURE 11 A, Proposed heterogeneous, two-layer model of the GWO dielectric. The chemical identification of the grain and grain boundaries are as indicated. B, Variation of the real part of the dielectric constant with W-concentration. The data shown is at room temperature. C, Variation of the real part of the dielectric constant with W-concentration. The data shown is at the highest temperature of the measurement (500°C). It is evident from the data shown in B and C, that the effect of W-doping on the dielectric constant is significant

active and the frequency of electron hopping frequency between the metal ions of variable valence states is observed to be at a lower level. This explains the lower conductivity of materials at lower frequency. However, as the frequency of the applied field increases, the GWO grains (interior) become more active. These highly active grains facilitate electron hopping between the same metal ions of variable valence state and, thereby, increases the hopping frequency. As a result, the electrical conductivity increases gradually with increasing frequency. This is clearly seen in frequency dependent electrical characteristics (Figure 10) of GWO dielectric materials. Having understood about the dielectric properties of GWO materials, it is imperative to shed light on their potential benefits, at least in the context of utilizing Ga_2O_3 based mixed oxides. Ga_2O_3 doping or mixed oxides are commonly used to design novel dielectric materials, particularly those ceramic compositions without any volatile elements such as Li or Na, for modern wireless communication devices, such as cellular phones, resonators, filters and oscillators in microwave integrated circuits.[73-75] Therefore, in addition to the traditional properties and applications, the present work on the dielectric properties of Ga_2O_3 and $Ga_{2-2x}W_xO_3$ ceramics may be useful and provide a road map when considering the mixed oxide ceramics based on Ga_2O_3 for designing such materials.

4 | CONCLUSIONS

A wide range of capacitor devices were fabricated using the tungsten doped Ga_2O_3 (GWO) as dielectric and silver (Ag) as the metal electrodes of the capacitor. The electrical performance of the capacitor devices based on W-doped Ga_2O_3 ($Ga_{2-2x}W_xO_3$, $0.00 \leq x \leq 0.20$; GWO) dielectric materials were evaluated by comprehensively studying the dielectric properties and electrical transport mechanisms. The W-concentration strongly influences the dielectric properties of GWO. The significant effect of W-doping is, however, dominant for higher concentration of W, where there is a secondary phase formation leading to the Ga_2O_3-WO_3 composite. At $f = 1$ kHz, at room temperature, varying W-content (x) from 0.0 to 0.2 increases the GWO dielectric constant from ~9 to ~90. Further enhancement in the dielectric constant due to W-doping was evident in the dielectric studies as a function of temperature, 25°C to 500°C. While the dielectric constant is temperature independent until ~300°C, rapid increase in dielectric constant beyond 300°C indicates the contribution from interfacial polarization to the enhanced dielectric constant. Modified Debye model accounts for the frequency (10^3-10^6 Hz) dependent variation in the dielectric constant of GWO dielectrics. The fitting of the experimental data to the

modified Debye model yield a relaxation time of ~20 to 90 μs and a spreading factor of 0.39 to 0.65. We propose a two-layer heterogeneous model consisting of thick grains separated by very thin grain boundaries along with the formation of a Ga_2O_3-WO_3 composite to explain the remarkable effect of W-incorporation on the dielectric and electrical transport properties of Ga_2O_3. The results demonstrate that the structure, electrical and dielectric properties can be tailored by tuning W-content in the GWO compounds. We believe that this fundamental study of dielectric properties as a function of frequency, temperature and W concentration could be useful to initiate further studies on the doping effects of wide-band gap semiconductors and could be useful for designing dielectric materials for electronic, optoelectronic and high power electronic device applications. In addition to the traditional electronic and optoelectronic device, the present work on the dielectric properties of Ga_2O_3 and $Ga_{2-2x}W_xO_3$ ceramics may be useful and provide a road map when considering the mixed oxide ceramics based on Ga_2O_3 for application in advanced communications.

ACKNOWLEDGMENTS

The authors acknowledge, with pleasure, support from the National Science Foundation (NSF) with NSF-PREM grant #DMR-1827745. The authors also acknowledge the support from NSF INTERN Program, Mr. Vishal Zade to perform graduate research work to broaden the participation and excellence in the materials design and development, as outlined in DCL NSF 18-102 and are highly obliged.

PEER REVIEW INFORMATION

Engineering Reports thanks Jackie Nel and other anonymous reviewer(s) for their contribution to the peer review of this work.

CONFLICT OF INTEREST

The authors declare no potential conflict of interest.

AUTHOR CONTRIBUTIONS

Vishal Zade: Formal analysis; investigation; methodology; validation; writing-original draft. **Mohan R. Rajkumar:** Data curation; formal analysis; investigation; methodology; validation. **Ron Broner:** Investigation; methodology. **Chintalapalle V. Ramana:** Conceptualization; formal analysis; funding acquisition; investigation; methodology; supervision; writing-review and editing.

ORCID

Chintalapalle V. Ramana https://orcid.org/0000-0002-5286-3065

REFERENCES

1. Bredar AR, Chown AL, Burton AR, Farnum BH. Electrochemical impedance spectroscopy of metal oxide electrodes for energy applications. *ACS Appl Energy Mater*. 2020;3(1):98-66.
2. Millán J, Godignon P, Perpiñà X, Pérez-Tomás A, Rebollo J. A Survey of Wide Bandgap Power Semiconductor Devices. *IEEE Trans Power Electron*. 2013;29(5):2155-2163.
3. Bandi M, Zade V, Roy S, et al. Effect of titanium induced chemical inhomogeneity on crystal structure, electronic structure, and optical properties of wide band gap Ga2O3. *Cryst Growth Des*. 2020;20(3):1422-1433.
4. Li W-B, Zhou D, Xu R, Pang L-X, Reaney IM. BaTiO3–Bi(Li0.5Ta0.5)O3, lead-free ceramics, and multilayers with high energy storage density and efficiency. *ACS Appl Energy Mater*. 2018;1(9):5016-5023.
5. Ma M, Zhang D, Li Y, Lin R, Zheng W, Huang F. High-performance solar blind ultraviolet photodetector based on single crystal orientation Mg-alloyed Ga2O3 film grown by a nonequilibrium MOCVD scheme. *ACS Appl Electron Mater*. 2019;1(8):1653-1659.
6. Cambiasso J, Grinblat G, Li Y, Rakovich A, Cortés E, Maier SA. Bridging the gap between dielectric nanophotonics and the visible regime with effectively lossless gallium phosphide antennas. *Nano Lett*. 2017;17(2):1219-1225.
7. Ramana C, Baghmar G, Rubio EJ, Hernandez MJ. Optical constants of amorphous, transparent titanium-doped tungsten oxide thin films. *ACS Appl Mater Interfaces*. 2013;5(11):4659-4666.
8. Robertson J. Band offsets of wide-band-gap oxides and implications for future electronic devices. *J Vac Sci Technol, B: Microelectron Nanometer Struct–Process, Meas, Phenom*. 2000;18(3):1785-1791.
9. Pearton S, Abernathy C, Overberg M, et al. Wide band gap ferromagnetic semiconductors and oxides. *J Appl Phys*. 2003;93(1):1-13.
10. Edgar J. Prospects for device implementation of wide band gap semiconductors. *J Mater Res*. 1992;7(1):235-252.
11. Dong L, Jia R, Xin B, Peng B, Zhang Y. Effects of oxygen vacancies on the structural and optical properties of β-Ga2O3. *Sci Rep*. 2017;7:40160.

12. Higashiwaki M, Sasaki K, Kuramata A, Masui T, Yamakoshi S. Gallium oxide (Ga2O3) metal-semiconductor field-effect transistors on single-crystal β-Ga2O3(010) substrates. *Appl Phys Lett*. 2012;100(1):013504.
13. Guo D, Liu H, Li P, et al. Zero-power-consumption solar-blind photodetector based on β-Ga2O3/NSTO heterojunction. *ACS Appl Mater Interfaces*. 2017;9(2):1619-1628.
14. Mastro MA, Kuramata A, Calkins J, Kim J, Ren F, Pearton S. Perspective—opportunities and future directions for Ga2O3. *ECS J Solid State Sci Technol*. 2017;6(5):P356–P359.
15. Pearton S, Yang J, Cary PH IV, et al. A review of Ga2O3 materials, processing, and devices. *Appl Phys Rev*. 2018;5(1):011301.
16. Åhman J, Svensson G, Albertsson J. A Reinvestigation of β-Gallium Oxide. *Acta Crystallogr, Sect C: Cryst Struct Commun*. 1996;52(6):1336-1338.
17. Yoshioka S, Hayashi H, Kuwabara A, Oba F, Matsunaga K, Tanaka I. Structures and energetics of Ga2O3 polymorphs. *J Phys Condens Matter*. 2007;19(34):346211.
18. Areán CO, Bellan AL, Mentruit MP, Delgado MR, Palomino GT. Preparation and characterization of mesoporous γ-Ga2O3. *Microporous Mesoporous Mater*. 2000;40(1-3):35-42.
19. Peelaers H, Van de Walle CG. Brillouin zone and band structure of β-Ga2O3. *Phys Status Solidi B*. 2015;252(4):828-832.
20. Gogova D, Wagner G, Baldini M, et al. Structural properties of Si-doped β-Ga2O3 layers grown by MOVPE. *J Cryst Growth*. 2014;401:665-669.
21. Kuramata A, Koshi K, Watanabe S, Yamaoka Y, Masui T, Yamakoshi S. High-quality β-Ga2O3 single crystals grown by edge-defined film-fed growth. *Jpn J Appl Phys*. 2016;55(12):1202A1202.
22. Arora K, Goel N, Kumar M, Kumar M. Ultrahigh performance of self-powered β-Ga2O3 thin film solar-blind photodetector grown on cost-effective Si substrate using high-temperature seed layer. *Acs Photonics*. 2018;5(6):2391-2401.
23. Muhammed MM, Alwadai N, Lopatin S, Kuramata A, Roqan IS. High-efficiency InGaN/GaN quantum well-based vertical light-emitting diodes fabricated on β-Ga2O3 substrate. *ACS Appl Mater Interfaces*. 2017;9(39):34057–34063.
24. Zhang J, Han S, Cui M, et al. Fabrication and interfacial electronic structure of wide bandgap NiO and Ga2O3 p–n heterojunction. *ACS Appl Electron Mater*. 2020;2(2):456-463.
25. Ginley DS, Bright C. Transparent conducting oxides. *MRS Bull*. 2000;25(8):15-18.
26. Minami T. Transparent conducting oxide semiconductors for transparent electrodes. *Semicond Sci Technol*. 2005;20(4):S35–S44.
27. Zhang W, Naidu BS, Ou JZ, et al. Liquid metal/metal oxide frameworks with incorporated Ga2O3 for photocatalysis. *ACS Appl Mater Interfaces*. 2015;7(3):1943-1948.
28. Mallesham B, Roy S, Bose S. Crystal Chemistry, Band-Gap Red Shift, and Electrocatalytic Activity of Iron-Doped Gallium Oxide Ceramics. et al. *ACS Omega*. 2019.5 104–112.
29. Syed N, Zavabeti A, Mohiuddin M, et al. Sonication-assisted synthesis of gallium oxide suspensions featuring trap state absorption: test of photochemistry. *Adv Funct Mater*. 2017;27(43):1702295.
30. Manandhar S, Battu AK, Devaraj A, Shutthanandan V, Thevuthasan S, Ramana C. Rapid Response High Temperature Oxygen Sensor Based on Titanium Doped Gallium Oxide. *Sci Rep*. 2020;10(1):1-9.
31. Ogita M, Higo K, Nakanishi Y, Hatanaka Y. Ga2O3 thin film for oxygen sensor at high temperature. *Appl Surf Sci*. 2001;175-176:721-725.
32. Yang G, Jang S, Ren F, Pearton SJ, Kim J. Influence of high-energy proton irradiation on β-Ga2O3 nanobelt field-effect transistors. *ACS Appl Mater Interfaces*. 2017;9(46):40471–40476.
33. Higashiwaki M, Kuramata A, Murakami H, Kumagai Y. State-of-the-art technologies of gallium oxide power devices. *J Phys D Appl Phys*. 2017;50(33):333002.
34. Yang M, Sun C, Wang T, et al. Graphene-oxide-assisted synthesis of Ga2O3 nanosheets/reduced graphene oxide nanocomposites anodes for advanced alkali-ion batteries. *ACS Appl Energy Mater*. 2018;1(9):4708-4715.
35. Huang Y, Tang X, Wang J, et al. Two-dimensional Ga2O3/C nanosheets as durable and high-rate anode material for lithium ion batteries. *Langmuir*. 2019;35(42):13607–13613.
36. Idrees M, Batool S, Kong J, et al. Polyborosilazane derived ceramics - nitrogen sulfur dual doped graphene nanocomposite anode for enhanced lithium ion batteries. *Electrochim Acta*. 2019;296:925-937.
37. Nogales E, García JÁ, Mendez B, Piqueras J. Doped gallium oxide nanowires with waveguiding behavior. *Appl Phys Lett*. 2007;91(13):133108.
38. Peelaers H, Van de Walle C. Doping ofGa2O3 with transition metals. *Physical Rev B*. 2016;94(19):195203.
39. Rubio EJ, Ramana CV. Tungsten-incorporation induced red-shift in the bandgap of gallium oxide thin films. *Appl Phys Lett*. 2013;102(19):191913.
40. Rubio E, Mates T, Manandhar S, Nandasiri M, Shutthanandan V, Ramana C. Tungsten incorporation into gallium oxide: crystal structure, surface and interface chemistry, thermal stability, and interdiffusion. *J Phys Chem C*. 2016;120(47):26720–26735.
41. Manandhar S, Battu AK, Tan S, Panat R, Shutthanandan V, Ramana C. Effect of Ti doping on the crystallography, phase, surface/interface structure and optical band gap of Ga2O3 thin films. *J Mater Sci*. 2019;54(17):11526–11537.
42. Zade V, Mallesham B, Shantha-Kumar S, Bronson A, Ramana C. Interplaybetween Solubility Limit, Structure, and Optical Properties of Tungsten-Doped Ga2O3 Compounds Synthesized by a Two-Step Calcination Process. *Inorg Chem*. 2019.58 3707–3716.
43. Roy S, Mallesham B, Zade VB, et al. Correlation between structure, chemistry, and dielectric properties of iron-doped gallium oxide (Ga2–xFexO3). *J Phys Chem C*. 2018;122(48):27597–27607.
44. Dakhel A. Structural, optical, and opto-dielectric properties of W-doped Ga2O3 thin films. *J Mater Sci*. 2012;47(7):3034-3039.
45. Dakhel A. Investigation of opto-dielectric properties of Ti-doped Ga2O3 thin films. *Solid State Sci*. 2013;20:54-58.

46. Yao Y, Davis RF, Porter LM. Investigation of different metals as ohmic contacts to β-Ga2O3: comparison and analysis of electrical behavior, morphology, and other physical properties. *J Electron Mater*. 2017;46(4):2053-2060.
47. Yao Y, Gangireddy R, Kim J, Das KK, Davis RF, Porter LM. Electrical behavior of β-Ga2O3 Schottky diodes with different Schottky metals. *J Vac Sci Technol, B: Microelectron Nanometer Struct–Process, Meas, Phenom*. 2017;35(3):03D113.
48. Shan J-J, Li C-H, Wu J-M, Liu J-A, Chen A-N, Shi Y-S. Sintering behavior and microstructural evolution of the monodispersed β-gallium oxide micro-particles with different morphology and size. *Ceram Int*. 2017;43(18):16843–16850.
49. Takahashi M, Inoue N, Takeguchi T, Iwamoto S, Inoue M, Watanabe T. Synthesis of γ-Ga2O3–Al2O3 solid solutions by the glycothermal method. *J Am Ceram Soc*. 2006;89(7):2158-2166.
50. Díaz J, López I, Nogales E, Méndez B, Piqueras J. Synthesis and characterization of silicon-doped gallium oxide nanowires for optoelectronic UV applications. *J Nanopart Res*. 2011;13(5):1833-1839.
51. Cao C, Chen Z, An X, Zhu H. Growth and field emission properties of cactus-like gallium oxide nanostructures. *J Phys Chem C*. 2008;112(1):95-98.
52. Yu S, Zhang G, Carloni D, Wu Y. Fabrication, microstructure and optical properties of Ga2O3 transparent ceramics. *Ceram Int*. 2020.
53. Zhao Y, Frost RL, Martens WN. Synthesis and characterization of gallium oxide nanostructures via a soft-chemistry route. *J Phys Chem C*. 2007;111(44):16290–16299.
54. Hao X. A review on the dielectric materials for high energy-storage application. *J Adv Dielectr*. 2013;3(01):1330001.
55. Kolekar Y, Sanchez L, Ramana C. Dielectric relaxations and alternating current conductivity in manganese substituted cobalt ferrite. *J Appl Phys*. 2014;115(14):144106.
56. Rahman MT, Vargas M, Ramana C. Structural characteristics, electrical conduction and dielectric properties of gadolinium substituted cobalt ferrite. *J Alloys Compd*. 2014;617:547-562.
57. Manika GC, Psarras GC. SrTiO3/epoxy nanodielectrics as bulk energy storage and harvesting systems: the role of conductivity. *ACS Appl Energy Mater*. 2019;3(1):831-842.
58. Anderson J. C. Dielectrics. Chapman & Hall, England; 1964.
59. Yuan J-K, Yao S-H, Dang Z-M, Sylvestre A, Genestoux M, Bai J. Giant Dielectric Permittivity Nanocomposites: Realizing True Potential of Pristine Carbon Nanotubes in Polyvinylidene Fluoride Matrix through an Enhanced Interfacial Interaction. *J Phys Chem C*. 2011;115(13):5515-5521.
60. Bharathi KK, Ramana C. Improved electrical and dielectric properties of La-doped Co ferrite. *J Mater Res*. 2011;26(4):584-591.
61. Maxwell JC. *A Treatise on Electricity and Magnetism*. Oxford: Clarendon Press; 1873.
62. Koops C. On the dispersion of resistivity and dielectric constant of some semiconductors at audiofrequencies. *Phys Rev*. 1951;83(1):121-124.
63. Kakade SG, Ma Y-R, Devan RS, Kolekar YD, Ramana CV. Dielectric, complex impedance, and electrical transport properties of erbium (Er3+) ion-substituted nanocrystalline, cobalt-rich ferrite (Co1.1Fe1.9–xErxO4). *J Phys Chem C*. 2016;120(10):5682-5693.
64. Kao KC. *Dielectric Phenomena in Solids*. San Diego, California: Elsevier; 2004.
65. Cole KS, Cole RH. Dispersion and absorption in dielectrics I. alternating current characteristics. *J Chem Phys*. 1941;9(4):341-351.
66. Sun Z, Ma C, Wang X, et al. Large energy density, excellent thermal stability, and high cycling endurance of lead-free BaZr0.2Ti0.8O3 film capacitors. *ACS Appl Mater Interfaces*. 2017;9(20):17096–17101.
67. Zade V, Mallesham B, Roy S, Shutthanandan V, Ramana C. Electronic structure of tungsten-doped β-Ga2O3 compounds. *ECS J Solid State Sci Technol*. 2019;8(7):Q3111–Q3115.
68. Liu Y, Hou Y, Ji Q, et al. Significant enhancement of energy storage performances by regulating the dielectric contrast between adjacent layers in the heterostructural composites. *ACS Appl Energy Mater*. 2020;3(3):3015-3023.
69. Juarez-Perez EJ, Sanchez RS, Badia L, et al. Photoinduced giant dielectric constant in lead halide perovskite solar cells. *J Phys Chem Lett*. 2014;5(13):2390-2394.
70. Adler D, Feinleib J. Electrical and optical properties of narrow-band materials. *Phys Rev B*. 1970;2(8):3112-3134.
71. Fawzi AS, Sheikh A, Mathe V. Structural, dielectric properties and AC conductivity of Ni(1−x)ZnxFe2O4 spinel ferrites. *J Alloys Compd*. 2010;502(1):231-237.
72. Khan W, Naqvi AH, Gupta M, Husain S, Kumar R. Small polaron hopping conduction mechanism in Fe doped LaMnO3. *J Chem Phys*. 2011;135(5):054501.
73. Muhammad R, Iqbal Y, Reaney IM. Structure and microwave dielectric properties of La5−x Sr x Ti4+x Ga1−x O17 ceramics. *J Mater Sci*. 2015;50(9):3510-3516.
74. Nono MCA, Castro PJ, Rangel EGL, Mineiro SL. Ga_2O_3-doped ZnO-Nb_2O_5-TiO_2 dielectric resonators for terrestrial and space telecommunications applications. *Mater Sci Forum*. 2016;869:79-84.
75. Dar MI, Sampath S, Shivashankar S. Exploiting oriented attachment in stabilizing La3+-doped gallium oxide nano-spindles. *RSC Adv*. 2014;4(90):49360–49366.

How to cite this article: Zade VB, Rajkumar MR, Broner R, Ramana CV. Chemical composition tuning induced variable and enhanced dielectric properties of polycrystalline $Ga_{2-2x}W_xO_3$ ceramics. *Engineering Reports*. 2021;3:e12300. https://doi.org/10.1002/eng2.12300